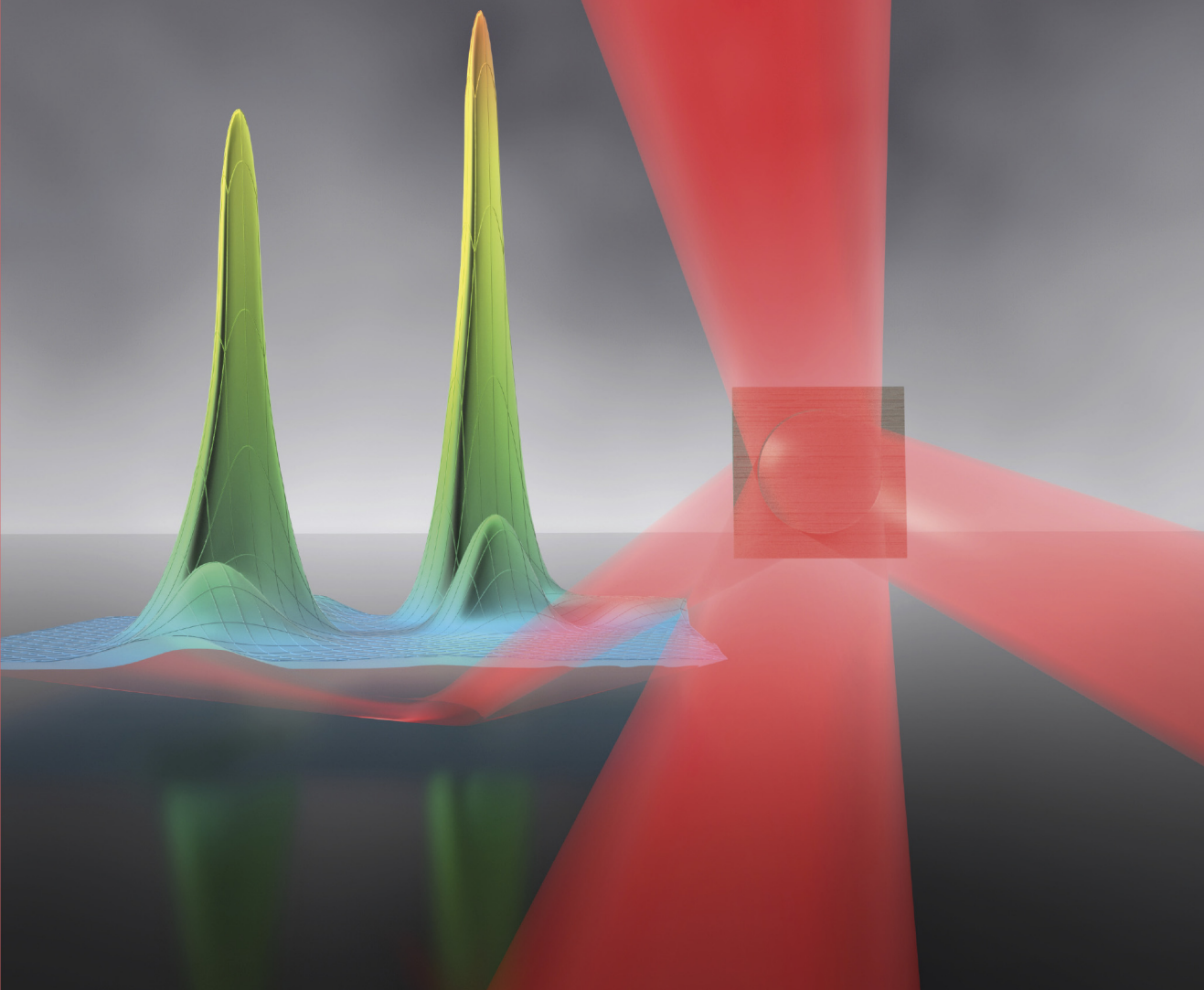


OXFORD



HEBIN LI
BACHANA LOMSADZE
GALAN MOODY
CHRIS SMALLWOOD
STEVEN CUNDIFF

Optical Multidimensional Coherent Spectroscopy

Optical Multidimensional Coherent Spectroscopy

Optical Multidimensional Coherent Spectroscopy

HEBIN LI

Florida International University

BACHANA LOMSADZE

Santa Clara University

GALAN MOODY

University of California Santa Barbara

CHRISTOPHER L. SMALLWOOD

San Jose State University

STEVEN T. CUNDIFF

University of Michigan

OXFORD
UNIVERSITY PRESS

OXFORD
UNIVERSITY PRESS

Great Clarendon Street, Oxford, OX2 6DP,
United Kingdom

Oxford University Press is a department of the University of Oxford.
It furthers the University's objective of excellence in research, scholarship,
and education by publishing worldwide. Oxford is a registered trade mark of
Oxford University Press in the UK and in certain other countries

© Hebin Li, Bachana Lomsadze, Galan Moody, Christopher L. Smallwood,
and Steven T. Cundiff 2023

The moral rights of the authors have been asserted

All rights reserved. No part of this publication may be reproduced, stored in
a retrieval system, or transmitted, in any form or by any means, without the
prior permission in writing of Oxford University Press, or as expressly permitted
by law, by licence or under terms agreed with the appropriate reprographics
rights organization. Enquiries concerning reproduction outside the scope of the
above should be sent to the Rights Department, Oxford University Press, at the
address above

You must not circulate this work in any other form
and you must impose this same condition on any acquirer

Published in the United States of America by Oxford University Press
198 Madison Avenue, New York, NY 10016, United States of America

British Library Cataloguing in Publication Data
Data available

Library of Congress Control Number: 2023930434

ISBN 978-0-19-284386-9

DOI: 10.1093/oso/9780192843869.001.0001

Printed and bound by
CPI Group (UK) Ltd, Croydon, CR0 4YY

Links to third party websites are provided by Oxford in good faith and
for information only. Oxford disclaims any responsibility for the materials
contained in any third party website referenced in this work.

We dedicate this book to our families who had to put up with our absence while we wrote it.

Preface

Ultrashort optical pulses, with duration ranging from a few picoseconds down to a few femtoseconds, have been used to study dynamics in matter since pulsed lasers were first developed in the 1960s. Indeed, this research area has been one of the drivers for improvements in the field of ultrafast optics, such as reductions in pulse duration. The field of using ultrashort light pulses to probe dynamical processes in matter is generally known as “ultrafast spectroscopy.”

Beginning in the late 1990s, the field of ultrafast spectroscopy underwent a revolution due to the introduction of multidimensional coherent spectroscopy based on concepts originally developed in nuclear magnetic resonance spectroscopy. Given their power, multidimensional coherent methods are becoming the dominant ultrafast spectroscopic techniques.

This book presents optical multidimensional coherent spectroscopy methods and their application to systems and materials that fall primarily within the field of physics. The systems include atomic vapors and solids—particularly semiconductors and semiconductor nanostructures. Multidimensional coherent spectroscopy in the infrared and visible spectral regions has been more extensively used to study molecules. As the application of multidimensional coherent spectroscopy to molecular systems has been covered by other books, we have chosen to not repeat that coverage here. Rather, we seek to broaden the coverage by addressing applications that are largely not covered elsewhere.

We begin by providing an introduction of multidimensional coherent spectroscopy for researchers in all fields, whether or not they have a background in ultrafast spectroscopy, or even in optical spectroscopy more generally. We then focus on the use of the technique to probe systems that are primarily of interest in the fields of physics and materials science. Our goal is to illustrate the information that multidimensional coherent spectroscopy can provide and its advantages over other methods. To do so, we focus on several exemplary materials, but also aim to illustrate the technique’s broader applicability.

Acknowledgements

We acknowledge all of those individuals who have worked or collaborated with us on developing and using multidimensional coherent spectroscopy including Diogo Almeida, Travis Autry, Wan Ki Bae, Manfred Bayer, Camelia Borca, Alan Bristow, Xingcan Dai, Matthew Day, Denis Karaickaj, Irina Kuznetsova, Xiaoqin (Elaine) Li, Albert Liu, Torsten Meier, Richard Mirin, Eric Martin, Shaul Mukamel, Gaël Nardin, Lazaro Padilha, Marten Richter, Mark Siemens, Kevin Silverman, Rohan Singh, Bo Sun, Takeshi Suzuki, Peter Thomas, Andreas Wieck and Tianhao Zhang. STC would like to acknowledge the sustained funding for research on this topic from the DOE Atomic, Molecular and Optical Science program and NSF funding through the JILA Physics Frontier Center.

Table of symbols

Symbol	Description	Section
A	cross-sectional interaction area	3.1
a_0	Bohr radius	5.3
a_B	exciton Bohr radius	9.1
\hat{B}/\hat{B}^\dagger	exciton annihilation/creation operator	5.3
C	probability amplitude	1.4
C_i	i^{th} London dispersion coefficient	5.3
c	speed of light in vacuum	1
D	spatial diffusion coefficient	1.3
$\mathcal{D}_\alpha(x, y, z)$	double-sided Feynman diagram equation	3.1
$E(t)$	total electric field in the time domain	1.2
$\hat{E}(t)$	complex-valued, slowly varying component of $E(t)$	1.2
$\tilde{E}(t)$	phasor description of E	2.3.3
E_0	real-valued electric field amplitude	1.2
E_B	biexciton energy	9.1
E_e	single-particle electron energy	9.1
E_h	single-particle hole energy	9.1
E_n	energy difference between two quantum states	1
E_{signal}	radiated electric field from polarization	2.3.3
E_X	exciton energy	9.1
$\mathcal{F}\{\dots\}$	Fourier transform operation	1.2
$\mathcal{E}(\omega)$	total electric field in the frequency domain	1.2
\mathcal{E}_0	electric field pulse area	1.2
f_0	comb offset frequency	6.1
f_{CE}	carrier-envelope offset frequency	4.4
f_n	frequency of n^{th} comb tooth	6.1
f_{rep}	laser repetition rate	4.4
$G(\omega)$	Fourier transform of $g(t)$ into the frequency domain	3.2
$g(t)$	Gaussian distribution function in the time domain	3.10
H	Hamiltonian operator of a system	1.4
H_0	unperturbed Hamiltonian operator of a system	1.4
h	Planck's constant, $h = 6.62607015 \times 10^{-34}$ J·s	1
\hbar	reduced Planck constant, $\hbar = h/2\pi$	1.4
I	optical intensity	1.2
I_{SI}	spectral interferogram intensity	4.3
\mathcal{I}	electric field power spectrum in the frequency domain	1.2
J_{mn}	one-exciton coupling strength between excitons m and n	5.3
K_{mn}	two-exciton coupling parameter	5.3

x *Table of symbols*

k	wavevector of light, $k = 2\pi/\lambda$	1.1
L	sample length	1.3
L_B	potential barrier width	9.1
L_c	laser cavity length	6.1
L_{min}	minimum potential barrier width for confinement	9.1
m_c	conduction band effective mass	7.1
m_e	electron mass	7.1
m_{hh}	heavy hole band effective mass	7.1
m_{lh}	light hole valence band effective mass	7.1
N	integer number pulses, data points, etc.	4.4
\mathcal{N}	particle density	5
N_p	number of particles	5.4
n	refractive index	1.1
$\langle \hat{O} \rangle$	expectation value of operator \hat{O}	1.4
P	dielectric polarization density	1.1
P_ψ	probability of being in state $ \psi\rangle$	1.4
$Q(x)$	probability distribution function	3.2
R	inter-atomic separation distance	5.3
r_c	correlation parameter	6.4
T	delay between second and third pulses	1.3
T_0	optical transmission	1.3
T_1	excited state population lifetime	3.1
T_2	excited/ground state coherence time	3.1
T_2^*	ensemble dephasing time	3.2
T_{rep}	laser repetition period	4.4
t	signal emission time	1.3
V	interaction Hamiltonian	1.4
$V(R)$	long-range atomic interaction potential	5.4
V_0	potential barrier height	9.1
v_{gr}	group velocity	6.1
v_{ph}	phase velocity	6.1
v_s	translation stage velocity	4.4
W	population inversion between quantum states	1.4
X_{hh}	heavy hole exciton	7.1
X_{lh}	light hole exciton	7.1
α_0	absorption coefficient	1.3
β	optical frequency chirp parameter	1.2
Δ_1	singly excited state interaction shift	6.4
Δ_2	doubly excited state interaction shift	6.4
ΔB	biexciton binding energy	9.1
ΔT	change in optical transmission	1.3

$\Delta\phi_{ce}$	carrier-envelope phase-slip	6.1
ΔX	exciton binding energy	7.1
$\delta(t)$	Dirac delta function	2.3.1
δt	temporal intensity pulse duration	1.2
δt_e	temporal intensity e^{-1} half width	1.2
δt_{e2}	temporal intensity e^{-2} half width	1.2
δt_{FWHM}	temporal intensity full-width at half maximum	1.2
δU	spectral intensity bandwidth in energy	1.2
$\delta\alpha_0$	change in absorption coefficient	1.3
$\delta\kappa$	spectral intensity bandwidth in wavenumbers	1.2
$\delta\lambda$	spectral intensity bandwidth in wavelength	1.2
$\delta\nu$	spectral intensity bandwidth in frequency	1.2
$\delta\omega$	spectral intensity bandwidth in angular frequency	1.2
$\delta\omega_e$	spectral intensity e^{-1} half width	1.2
$\delta\omega_{e2}$	spectral intensity e^{-2} half width	1.2
$\delta\omega_{\text{FWHM}}$	spectral intensity full-width at half maximum	1.2
ϵ_0	vacuum permittivity	3.1
Γ	relaxation operator	1.4
Γ_{10}	excited state population decay rate	3.1
Γ_{gr}	grating relaxation rate	1.3
Γ_{pop}	population relaxation rate	1.3
γ	dephasing rate / homogeneous linewidth	1.3
γ_{10}	excited/ground state decoherence rate	3.1
γ_{ij}	imaginary part of resonance frequency between states i and j	2.3.1
γ^{ph}	pure dephasing rate	1.4
γ_t	single quantum dephasing rate	6.4
γ_τ	double quantum dephasing rate	6.4
$\Theta(x)$	Heaviside step function	1.3
θ	angle between beams 1 and 2	1.3
ϑ	Bloch sphere polar angle	1.5
Λ	spatial grating period	1.3
λ	wavelength of light in vacuum	1
μ	electric dipole moment	1.4
ν	frequency of light	1
ν^*	difference frequency between signal and CW reference laser	4.4
π	mathematical constant $\pi \approx 3.1415$	1.1
ρ	density matrix operator	1.4
σ	N -particle spectral distribution width	3.2
τ	delay between first and second pulses	1.3
τ_{ex}	two-level transition excited-state lifetime	1.3
χ	electric susceptibility	1.1

xii *Table of symbols*

ϕ	optical phase	1.2
$\phi_{S,R}$	phase of signal/reference electric field	4.3
φ	Bloch sphere azimuthal angle	1.5
$ \psi\rangle$	quantum mechanical wave function	1.4
Ω_{ij}	complex resonance frequency between states i and j	2.3.1
Ω_r	Rabi frequency	1.4
ω	optical angular frequency	1.2
ω_0	resonant angular frequency of an optical transition	3.2.1
ω_c	carrier angular frequency of a laser	1.2
ω_{ij}	real part of resonance frequency between states i and j	2.3.1
ω_t	frequency conjugate to emission time, t	3.1
ω_τ	frequency conjugate to coherence time, τ	3.1

Table of acronyms

Acronym	Description
2DCS	two-dimensional coherent spectroscopy
2DES	two-dimensional electronic spectroscopy
AOM	acousto-optic modulator
BS	beamsplitter
°C	degrees Celsius
c.c.	complex conjugate
CAD	computer-aided design
CB	conduction Band
CCD	charge-coupled device
CP	compensation plate
CQD	colloidal quantum dot
CVD	chemical vapor deposition
CW	continuous wave
DBR	distributed Bragg reflector
DCM	dichroic mirror
DCS	dual-comb spectroscopy
DDS	direct-digital synthesizer
DFT	discrete Fourier transform
DQW	double quantum well
DSP	digital signal processor
EID	excitation induced dephasing
EIS	excitation induced shift
ESE	excited-state emission
FFT	fast Fourier transform
FPGA	field programmable gate array
FTIR	Fourier-transform infrared
FWHM	full-width at half-maximum
GNE	gold nanoelectrode
GSB	ground-state bleaching
HeNe	helium-neon
hh	heavy hole
HWP	half-wave plate
IFQD	interface fluctuation quantum dots
IR	infrared
lh	light hole
LO	local oscillator
LP	lower polariton

MAPI	Methylammonium Lead Iodide
MBE	molecular beam epitaxy
MDCS	multi-dimensional coherent spectroscopy
MONSTR	multidimensional optical nonlinear spectrometer
MQC	multi-quantum coherence
NA	numerical aperture
NMR	nuclear magnetic resonance
NW	narrow well
OD	optical density
PBS	polarizing beamsplitter
PL	photoluminescence
PLE	photoluminescence excitation
PZT	piezoelectric transducer
QD	quantum dot
QW	quantum well
RBM	radial breathing mode
RF	radio frequency
SAQD	self-assembled quantum dot
SERS	surface-enhanced Raman spectroscopy
SNR	signal-to-noise ratio
SR-TFWM	spectrally resolved transient four-wave mixing
STM	scanning tunneling microscope
SWNT	single-walled carbon nanotube
TBP	time-bandwidth product
TC	lock-in amplifier time constant
TCS	tri-comb spectroscopy
TFWM	transient four-wave mixing
TI-TFWM	time-integrated transient four-wave mixing
TMD	Transition Metal Dichalcogenide
Tr	trace of a linear operator
TR-TFWM	time-resolved transient four-wave mixing
UP	upper polariton
VB	valence band
WW	wide well
ZPL	zero phonon line

Contents

1	Basics of ultrafast spectroscopy	1
1.1	Basics of spectroscopy: linear versus nonlinear	2
1.2	Ultrashort pulses	6
1.3	Ultrafast nonlinear/coherent spectroscopy	10
1.4	The density matrix	15
1.5	Bloch sphere representation of quantum states	20
2	Introduction to multidimensional coherent spectroscopy	23
2.1	Concepts of multidimensional coherent spectroscopy	24
2.2	Spectrum classification	29
2.3	Density matrix formalism and double-sided Feynman diagrams	32
2.4	Phase matching	43
2.5	Two-dimensional infrared (2D IR) spectroscopy	44
3	Interpretation of multidimensional coherent spectra	45
3.1	Isolated two-level system	45
3.2	Inhomogeneously broadened ensemble of two-level systems	49
3.3	Coherent coupling signatures	55
3.4	Incoherent coupling signatures	57
3.5	Doubly excited states and many-body interactions	58
3.6	Double-quantum spectra	62
3.7	Zero-quantum spectra	65
3.8	Three-dimensional coherent spectroscopy	67
3.9	Nonrephasing pathways and purely absorptive spectra	67
3.10	Finite-pulse effects	68
4	Experimental implementations	77
4.1	Experimental requirements and considerations	77
4.2	Overview of experimental approaches	80
4.3	Actively stabilized box geometry	81
4.4	Phase modulated collinear geometry	89
4.5	Comparison of different approaches	97
4.6	Data analysis	97
5	Multidimensional coherent spectroscopy of atomic ensembles	101
5.1	Single- and zero-quantum 2D spectra of atomic vapors	102
5.2	MDCS in optically thick samples	108
5.3	Probing many-body interactions with double-quantum 2D spectroscopy	112

5.4	Probing many-body correlations with multi-quantum 2D spectroscopy	121
6	Frequency comb-based multidimensional coherent spectroscopy	127
6.1	Introduction to frequency combs and dual-comb spectroscopy	128
6.2	Frequency comb-based four-wave-mixing spectroscopy	130
6.3	Frequency comb-based single-quantum 2D spectroscopy	135
6.4	Frequency comb-based double-quantum 2D spectroscopy	139
6.5	Tri-comb spectroscopy	144
7	Two-dimensional spectroscopy of semiconductor quantum wells	151
7.1	Introduction to semiconductor optics	152
7.2	Many-body signatures in one-quantum 2D spectra	154
7.3	Many-body signatures in double- and multi-quantum 2D spectra	161
7.4	Two-dimensional spectroscopy of coupled quantum wells	165
7.5	Quantum well exciton-polaritons in microcavities	168
8	Three-dimensional coherent spectroscopy	171
8.1	Fifth-order 3D infrared spectroscopy	172
8.2	Fifth-order 3D electronic spectroscopy	173
8.3	Third-order 3D electronic spectroscopy	174
8.4	3D coherent frequency domain spectroscopy	191
9	Two-dimensional spectroscopy of semiconductor quantum dots	193
9.1	Optical and electronic properties of quantum dots	193
9.2	2D coherent spectroscopy of GaAs quantum dots	197
9.3	2D spectroscopy of self-assembled In(Ga)As quantum dots	202
9.4	Coherent control of quantum dots	205
9.5	Two-dimensional spectroscopy of colloidal quantum dots	207
10	Two-dimensional spectroscopy of atomically thin 2D materials	213
10.1	Introduction to 2D materials	213
10.2	Homogeneous linewidth in 2D materials	214
10.3	Valley coherence and coupling in 2D materials	217
11	Other applications of multi-dimensional coherent spectroscopy in Physics	223
11.1	Semiconducting carbon nanotubes	223
11.2	Color centers in diamond	225
11.3	Perovskite materials	228
12	New trends in multidimensional coherent spectroscopy	235
12.1	Broadening the spectral range: from terahertz to x-rays	235
12.2	Improving the spatial resolution	237

12.3 Multidimensional spectroscopy with quantum light	239
12.4 Photoemission-detected MDCS	240
Figure Credits	243
References	245
Index	279

1

Basics of ultrafast spectroscopy

Starting from Issac Newton's use of a prism to observe the spectrum of sunlight, optical spectroscopists have been striving to further our understanding of matter by studying how it absorbs and emits light. Spectroscopic techniques remained fundamentally unchanged for centuries compared to Newton's method. Light was dispersed by a prism or diffraction grating and the intensity was measured as a function of angle, which can be mapped into wavelength. Changes in the spectral intensity can be related to either inherent properties of the source or the light passing through a medium that absorbs at specific wavelengths. The absorption or emission wavelength can be converted to a frequency through $c = \lambda\nu$ where c is the speed of light, λ is the wavelength of the light and ν is its frequency. Using the quantum mechanical relation between energy, E_n , and frequency, $E_n = h\nu$, where h is Planck's constant, the frequency can be understood as the energy difference between two quantum states such as electronic or vibrational states.

Before the invention of the laser, spectroscopic measurements were all performed in the linear regime where the material properties are independent of the intensity of the light. In this regime the electric field of the light is weak compared to the internal fields of the atom or molecule. A laser can produce light that is no longer weak compared to the internal fields of an atom or molecule, thus the invention of the laser brought the field of optical spectroscopy into a new era of nonlinear spectroscopy. In the nonlinear regime, the material properties are no longer independent of the light intensity, signals scale with a higher power of the laser intensity, and two laser beams can interact in a sample. For instance, a strong pump beam can saturate an absorption resonance and thus increase the transmission of a weaker probe beam. Also, wave-mixing of multiple light fields in the sample can lead to a signal beam with an entirely new direction and frequency.

Optical spectroscopic measurements can also be made not as a function of wavelength but rather of time. Time-domain spectroscopy is analogous to the idea of a stroboscope, in that short flashes of light can capture stop-action images of ultrafast dynamics such as a chemical reaction or charge carriers relaxing in a solid. Measurements made in the time domain using laser pulses can be converted into frequency-domain spectra using a Fourier transform. In general, the time-domain spectra can be functions of multiple time delays, so the resulting frequency-domain spectra are functions of multiple frequencies and thus are multidimensional. The concept of multidimensional Fourier transform spectroscopy was developed in nuclear magnetic resonance (NMR) [108] and is now transforming the field of ultrafast laser spectroscopy.

2 Basics of ultrafast spectroscopy

Multidimensional coherent spectroscopy has a number of advantages over other types of spectroscopy, including one-dimensional methods and multidimensional methods that are not coherent. At the same time, multidimensional coherent spectroscopy is challenging to experimentally implement in the optical portion of the electromagnetic spectrum due to the need to use phase-related light pulses to excite the sample and to measure the phase of the emitted light signals.

To set the stage before discussing multidimensional coherent methods, in this chapter we will review several ultrafast spectroscopic methods, both because they serve as the foundation from which multidimensional coherent methods were developed, and they provide context for describing the advantages of multidimensional coherent methods. In Chapter 2 we will introduce the basic concepts involved in multidimensional coherent spectroscopy, followed by an in-depth discussion of how to interpret multidimensional coherent spectra in Chapter 3. Chapter 4 will review several experimental implementations, describing how each overcomes the aforementioned challenges.

1.1 Basics of spectroscopy: linear versus nonlinear

The field of spectroscopy involves measuring a spectrum that displays the frequency (spectral) dependence of the interaction between matter and electromagnetic radiation. The electromagnetic radiation may be incident on the matter from an external source, or it may be emitted by the matter. In this book, we will discuss the former case.

When an electromagnetic field is incident on matter, it displaces the electrons or ions in the matter from their equilibrium positions, producing a polarization in the matter that in turn radiates a new electromagnetic field. Treating the polarization as a driving term in Maxwell's equations and taking the far-field limit gives the result that the phase of the reradiated field lags the phase of the polarization by 90° (a factor of i in complex phasor notation). The interference of this reradiated field with the incident field results in modification of the field due to propagation through the matter, which is usually attributed to material properties such as an index of refraction or absorption.

In linear spectroscopy, the incident electromagnetic field is weak and the induced polarization is linearly proportional to the incident field. For a continuous wave (CW) incident field, the polarization will have the same frequency and wavevector as the incident field. However, the phase of the polarization with respect to the incident field depends on frequency if resonances are present in the material. First, we consider only a single resonance as the simplest example.

If the frequency of the incident field is significantly below the resonant frequency, then the induced polarization will be in-phase with the incident field and the reradiated field will be 90° out of phase in the far field due to aforementioned far-field phase lag. Since the polarization has the same wavevector as the incident field, the reradiated field will propagate in the same direction, so a detector placed after the sample will detect the sum of the incident field and the reradiated field. If the reradiated field is weak compared to the incident field, the dominant result will simply be a phase shift of the transmitted field compared to the incident field, as illustrated in Fig. 1.1(a) [note that $e^{ikx} + i\delta e^{ikx} \approx e^{i(kx+\delta)}$ for small values of δ , where $k = 2\pi n/\lambda$]. This phase shift is consistent with a transparent material with an index of refraction n .

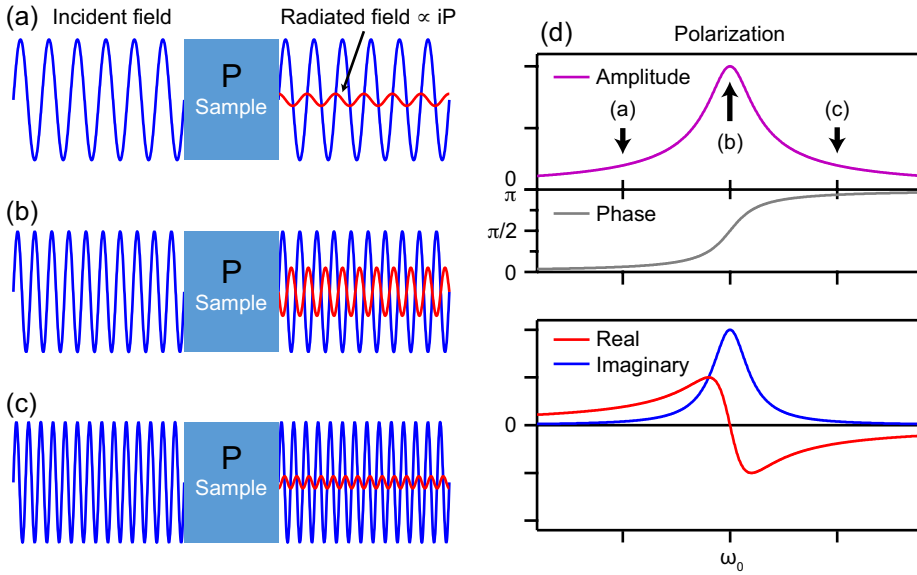


Fig. 1.1 Sketch of linear spectroscopy showing incident fields and reradiated fields in the vicinity of an optical resonance. **(a)** Below resonance. **(b)** On resonance. **(c)** Above resonance. **(d)** Frequency dependence of the complex polarization, in terms of amplitude and phase (top) and real and imaginary quadratures (bottom).

If the frequency of the incident field is tuned so that it is on the resonance in the sample, the phase of the polarization will lag that of the incident field by 90° . Together with the far-field phase shift, the net result will be that the reradiated field will be 180° out of phase with the incident field and they will experience destructive interference when measured together, as sketched in Fig. 1.1(b). This destructive interference means that a lower transmitted intensity is measured, as expected, because the incident field is now being absorbed by the sample since it is on resonance.

Tuning the frequency of the incident field to be above resonance results in a situation similar to below resonance, just a phase shift of the transmitted field, although the phase shift is in the opposite direction, as shown in Fig. 1.1(c).

Taken as a whole, this simplified picture of absorption spectroscopy is useful because it emphasizes the importance of the relative phase between the incident field and the induced polarization: it is all the difference between a material being transparent but causing a phase shift of the transmitted light and the material absorbing the light and resulting in less light being transmitted. The ability to measure the phase of the polarization with respect to the incident fields can be implemented in multidimensional coherent spectroscopy, and it yields important information about how the material is responding to the incident light.

The complete frequency dependence of the material polarization in the vicinity of the resonance is depicted in Fig. 1.1(d), divided into complex amplitude and phase components at top and into real and imaginary quadratures on bottom. The quadra-

4 *Basics of ultrafast spectroscopy*

ture depiction, in particular, exhibits a number of important features that will serve as useful reference points for the nonlinear multidimensional spectra that will be discussed in much of the rest of this book. As mentioned above, when the polarization signal is both small and primarily real-valued, the dominant effect on the emitted signal is a change in phase. In fact, the real part of the polarization remains closely connected to phase shifts in the optical field regardless of what imaginary part if the overall reradiated signal amplitude remains small in comparison to the incident field. Because these phase shifts are different for light at different frequencies, the quadrature is very often referred to in spectroscopy literature as the polarization's "dispersive" component. Likewise, the polarization's imaginary component bears a strong resemblance to the material's absorption properties and as such is frequently termed the signal's "absorptive" component. In terms of the reradiated field—which is the most commonly examined quantity in MDCS—the dispersive component shifts into the signal's imaginary quadrature and the absorptive component shifts into the real quadrature.

This discussion has described a simple spectroscopy experiment, namely sweeping the frequency of an electromagnetic field incident on a sample and measuring the transmitted intensity. If a dip in the transmitted intensity is observed at a specific frequency it indicates the presence of resonance; the width of the resonance characterizes the damping of the resonance. However, there are important ambiguities in linear spectra, namely the inability to distinguish between homogeneous and inhomogeneous broadening and the inability to determine if two resonances are coupled or uncoupled.

Typically the sample is an ensemble of many systems, whether they are atoms undergoing electronic transitions, molecules undergoing vibrational transitions, or nuclei flipping their spins. If all the systems in the ensemble are identical, i.e., they have the same resonant frequency and same linewidth, the ensemble is designated as being "homogeneously broadened"; however, this may not necessarily be the case. In particular, there may be a distribution of resonant frequencies due to effects such as the Doppler shift in a vapor, random crystal fields in an ion-doped solid or structural disorder in a nanostructure. In this case, the linewidth of the measured resonance may have nothing to do with the linewidth of the individual members of the ensemble, but rather reflects the distribution of resonance frequencies. This case is known as "inhomogeneous broadening."

The linear spectrum of an inhomogeneously broadened ensemble will have a resonance feature (the absorption "line") that has a width that is characteristic of the inhomogeneous distribution, not the damping of the individual members of the ensemble. While both are useful to know, they provide quite different information. The width in the absence of the inhomogeneous broadening, often called the "homogeneous width" provides information about processes that interrupt the oscillations, for example collisions and radiative decay.

There is also an ambiguity in linear spectroscopy if two resonances are observed in a linear spectrum. There are two possible situations. One possibility is that the sample is heterogeneous, i.e., a mixture of two species with different resonance frequencies. The other possibility is that it is pure, i.e., a single substance, but that substance has two transitions. A good example of this latter case would be the D_1 and D_2 lines in the alkali metals, which correspond to the single outer electron making a transition

to ground $S_{1/2}$ state the $P_{1/2}$ and $P_{3/2}$ states. Linear spectroscopy cannot distinguish between these two possibilities.

These ambiguities can be resolved by using some form of nonlinear spectroscopy. In nonlinear spectroscopy, as the intensity of the excitation field is increased, the dielectric polarization $P(\omega)$ of a material is no longer linearly proportional to the incident field, but rather higher-order terms must be considered. In the frequency domain, we can describe this in terms of a power series expansion of $P(\omega)$ as function of electric field strength $\mathcal{E}(\omega)$ as

$$P[\mathcal{E}(\omega)] = \epsilon_0 \left[\chi^{(1)}\mathcal{E} + \chi^{(2)}\mathcal{E}^2 + \chi^{(3)}\mathcal{E}^3 + \chi^{(4)}\mathcal{E}^4 + \dots \right], \quad (1.1)$$

where the constant ϵ_0 is the vacuum permittivity and the coefficients $\chi^{(n)}(\omega)$ describe electric susceptibility parameters of the material at each of the different orders n . Linear spectroscopy corresponds to the situation where all the terms $\chi^{(n)}\mathcal{E}^n$ for $n > 1$ are small enough to be neglected, resulting in the relationship $P(\omega) = \epsilon_0\chi^{(1)}(\omega)\mathcal{E}(\omega)$. Of course, this approximation depends on the strength of \mathcal{E} , because for large enough \mathcal{E} , the \mathcal{E}^n factor can make $\chi^{(n)}\mathcal{E}^n > \chi^{(1)}\mathcal{E}$, no matter how small the ratio $\chi^{(n)}/\chi^{(1)}$. It is possible to show that for inversion symmetric systems, the second-order term in the expansion of Eq. (1.1), and indeed all of the even-valued higher-order terms, must be identically equal to zero.¹ Hence, in delving into the world of nonlinear spectroscopy, it is often the $\chi^{(3)}$ term that is actually the most important element governing nonlinear corrections to the polarization as a whole, and so it is upon this term that we will most heavily concentrate our attention in this book.

To understand how nonlinear spectroscopy can resolve the ambiguities in a linear spectrum, it is easiest to consider a simple frequency-domain method known as “spectral hole burning.” In spectral hole burning, a continuous wave (CW) “pump” laser excites the sample, saturating its absorption. A second laser is then scanned to measure the absorption of the sample. If the sample is homogeneously broadened, the absorption of the entire line simply decreases. However, if it is inhomogeneously broadened, then the sub-ensemble that is resonant with the pump laser is most strongly saturated. In this case, the measured absorption spectrum is unchanged, except in the spectral region close to the pump, where the absorption is decreased, known as “burning a hole.” The width of the spectral hole is proportional to the homogeneous width. Thus the observation of spectral hole burning shows that the system is inhomogeneously broadened and the width gives the homogeneous width.

Similarly, if two resonances are present in the spectrum, tuning the pump laser to one resonance and probing the other can determine if they are coupled. If they are coupled, then this situation will result in a change in the absorption, whereas if they are uncoupled it will not. This example was based on using CW lasers. Although there are some implementations of optical multidimensional coherent spectroscopy based on this approach [55–57, 443], most are based on using mutually coherent pulses and scanning their delays.

A time-domain multidimensional coherent spectroscopy (MDCS) measurement is made by illuminating a sample with a series of light pulses and measuring a signal

¹See, for example, *Nonlinear Optics*, by Robert W. Boyd [40].

from the sample as a function of the delays between the pulses. Typically the pulses have duration of a few picoseconds or less, which is considered the domain of “ultrafast optics,” where traditional photodetectors are too slow to directly measure the pulse duration. Due to their short duration, such pulses intrinsically have broad spectral bandwidth, thus spectral features can be measured without tuning them spectrally, but rather by spectrally resolving them. While this can be done using traditional spectrometers, it can also be realized using Fourier transform methods. Some MDCS approaches only use Fourier transforms, whereas others use a combination of Fourier transforms and a spectrometer to spectrally resolve the signal.

Before we introduce MDCS, we need to briefly review the properties of ultrashort pulses and introduce less related forms of spectroscopy that are based on ultrashort optical pulses.

1.2 Ultrashort pulses

A short optical pulse passing through a fixed point in space can be described by its electric field in the time domain

$$\begin{aligned} E(t) &= |\hat{E}(t)| \cos(-\omega_c t + \phi(t)) \\ &= \frac{1}{2} \hat{E}(t) e^{-i\omega_c t} + \text{c.c.}, \end{aligned} \quad (1.2)$$

where ω_c is the carrier frequency, and where $\phi(t)$ is a time-dependent phase. The second line of the equation is expressed in phasor notation, with the complex-valued amplitude $\hat{E}(t) = |\hat{E}(t)|e^{i\phi(t)}$, and with the abbreviation “c.c.” standing for “complex conjugate.” For the discussion throughout the first three chapters of this book, we ignore the fact that light has a polarization, and thus treat the electric field as a scalar. Note that the choice of ω_c is in principle arbitrary; the same pulse could be described using a different ω_c by adjusting the time dependence of the amplitude coefficients to include linearly ramping phase factors. Typically, however, ω_c is chosen to eliminate a linear ramp in $\phi(t)$. Throughout this book we use a caret (\hat{X}) placed over the top of a function X to indicate a value assumed to vary “slowly” in time (i.e., to be nearly constant over several periods of the optical frequencies).

Although slow in comparison to the carrier oscillations, time dependence of the amplitude factor $\hat{E}(t)$ as introduced in Eq. (1.2) is still required to shape the light into a pulse. Writing out the amplitude and phase components of $\hat{E}(t)$ explicitly and then expressing them in terms of optical intensity $I(t) \equiv n\epsilon_0 c \langle E(t)^2 \rangle$ leads to

$$E(t) = \frac{1}{2} \sqrt{\frac{2I(t)}{n\epsilon_0 c}} e^{-i[\omega_c t - \phi(t)]} + \text{c.c.}, \quad (1.3)$$

where n is refractive index, ϵ_0 is the vacuum permittivity, c is the speed of light, and the angle brackets in the definition of intensity specify the time average over an optical period. As shown in Fig. 1.2, the pulse described using Eq. (1.3) can be visualized as an oscillating carrier, of frequency ω_c , under an envelope proportional to $\sqrt{I(t)}$. The constant in the phase factor $\phi(t)$ allows the possibility of a shift in

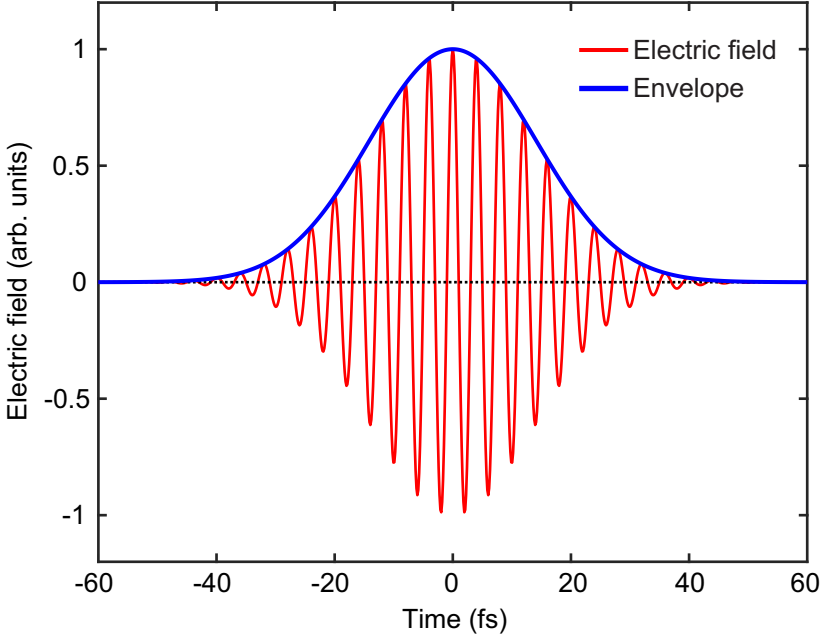


Fig. 1.2 The electric field (solid red line) and the envelope (blue line) of an ultrafast pulse.

alignment between the ripples of the carrier and the overall envelope position, known as the “carrier-envelope phase.”

One reasonable mathematical description of an ultrafast pulse is Gaussian. The envelope of a Gaussian pulse is

$$\hat{E}(t) = E_0 e^{-\frac{t^2}{(\delta t_{e2})^2}} \quad (1.4)$$

where E_0 is the (real-valued) amplitude and the parameter δt_{e2} describes pulse duration. The pulse intensity associated with Eq. (1.4) is

$$I(t) \propto |\hat{E}(t)|^2 = E_0^2 e^{-\frac{2t^2}{(\delta t_{e2})^2}} = E_0^2 e^{-\frac{t^2}{(\delta t_{e2}/\sqrt{2})^2}}, \quad (1.5)$$

which demonstrates that for a Gaussian pulse, the duration parameter δt_{e2} corresponds to the half width at which the pulse intensity drops to $1/e^2$ (13.5%) of its peak. Beyond this, the equation shows that the pulse duration of the intensity function is a factor of $\sqrt{2}$ shorter than the pulse duration of the amplitude function. Although the $1/e^2$ half-width definition of pulse duration is common, the duration of a pulse can be defined according to any number of different conventions, including the intensity half width $1/e$ value (δt_e), the intensity full width at half maximum (FWHM) value (δt_{FWHM}), and various definitions associated with the intensity autocorrelation function. Thus, it is important to define the pulse duration carefully when introducing it as a parameter in order to avoid ambiguities. For Gaussian pulses, the duration parameters δt_e , δt_{e2} , and δt_{FWHM} are related to each other by

$$(\delta t_{\text{FWHM}}) = \sqrt{2 \ln 2} (\delta t_{e2}) = 2\sqrt{\ln 2} (\delta t_e). \quad (1.6)$$

However, the conversion factors relating the various width definitions are different for different pulse shapes.

An ultrashort pulse can also be described in the frequency domain where the electric field is written as a function of the angular frequency or frequency. The conversion between the time and frequency domains is performed by the Fourier Transform of the electric field (not the intensity), where the forward Fourier Transform

$$\mathcal{E}(\omega) = \int_{-\infty}^{\infty} E(t) e^{i\omega t} dt \quad (1.7)$$

converts from a time-domain signal, $E(t)$, to its frequency-domain representation, $\mathcal{E}(\omega)$, and the inverse Fourier transform

$$E(t) = \frac{1}{2\pi} \int_{-\infty}^{\infty} \mathcal{E}(\omega) e^{-i\omega t} d\omega. \quad (1.8)$$

converts the other direction, giving the time-domain waveform from the frequency-domain representation. Note that there differing conventions for the definition of the Fourier Transform with regards to the sign of the exponent in the kernel ($e^{i\omega t}$ versus $e^{-i\omega t}$) and normalization ($\frac{1}{2\pi}$ in front of the inverse Fourier transform versus $\sqrt{\frac{1}{2\pi}}$ in front of both the forward and inverse transforms). Throughout this book we will use the conventions given in Eqs. (1.7) and (1.8). The Fourier transform of Eq. (1.3) gives

$$\mathcal{E}(\omega) = \frac{1}{2} \sqrt{\frac{2\mathcal{I}(\omega - \omega_c)}{n\epsilon_0 c}} e^{i\phi(\omega - \omega_c)} + \frac{1}{2} \sqrt{\frac{2\mathcal{I}(-\omega - \omega_c)}{n\epsilon_0 c}} e^{-i\phi(-\omega - \omega_c)}. \quad (1.9)$$

The field in the frequency domain has both positive and negative frequencies. The two frequency components are actually equivalent, but required to make the signal real. We usually take only the positive frequency and center the pulse at zero frequency (i.e., expressed in the rotating frame) in complex phasor notation as

$$\mathcal{E}(\omega) = \frac{1}{2} \sqrt{\frac{2\mathcal{I}(\omega)}{n\epsilon_0 c}} e^{i\phi(\omega)}. \quad (1.10)$$

Here $\mathcal{I}(\omega)$ is the spectral intensity function and the frequency-domain phase is

$$\phi(\omega) = \arctan \left\{ \frac{\text{Im}[\mathcal{E}(\omega)]}{\text{Re}[\mathcal{E}(\omega)]} \right\}. \quad (1.11)$$

The phase calculated from Eq. (1.11) can only vary from $-\pi$ to π so there could be 2π phase jumps. We can unwrap the phase by adding or subtracting 2π to avoid phase jumps and have a continuous phase. The phase defined by Eq. (1.11) has no meaning when the intensity is zero. The phase is noisy when the intensity is small at the wings of spectrum, in which case the phase is usually not plotted. According to the Fourier

shift theorem, a delay in the time domain is a linear phase ramp in the frequency domain, i.e., $\mathcal{F}\{E(t - t_0)\} = \mathcal{E}(\omega)e^{i\omega t_0}$.

Applying the Fourier transform to the time-domain Gaussian pulse described by Eq. (1.4) gives the frequency-domain pulse in a frame rotating at the carrier frequency as

$$\mathcal{E}(\omega) = \sqrt{\pi}(\delta t_{e2})E_0e^{-\frac{(\delta t_{e2})^2\omega^2}{4}}. \quad (1.12)$$

The intensity spectrum of the pulse is

$$\mathcal{I}(\omega) = \frac{n\epsilon_0 c}{2}\pi(\delta t_{e2})^2E_0^2e^{-\frac{(\delta t_{e2})^2\omega^2}{2}} \propto E_0^2e^{-\frac{2\omega^2}{(2/\delta t_{e2})^2}}, \quad (1.13)$$

which demonstrates that the spectral profile of a time-domain Gaussian pulse is also a Gaussian. The $1/e^2$ half width intensity spectral bandwidth of this Gaussian is $(\delta\omega_{e2}) = 2/(\delta t_{e2})$.

As in the time-domain representation of the electric field, there are different kinds of conventions for describing spectral bandwidth, including the spectral intensity $1/e^2$ half width (δ_{e2}) , the spectral intensity $1/e$ half width $(\delta\omega_e)$, and the spectral intensity FWHM value $(\delta\omega_{\text{FWHM}})$. In similar fashion to the ways that time-domain pulse durations are related to each other, for Gaussian pulses these frequency-domain bandwidth descriptions are connected through the relationship

$$(\delta\omega_{\text{FWHM}}) = \sqrt{2\ln 2}(\delta\omega_{e2}) = 2\sqrt{\ln 2}(\delta\omega_e). \quad (1.14)$$

Different research fields also use different units in the frequency domain. The spectrum and bandwidth can be presented as a function of frequency (THz), angular frequency (rad/s), wavelength (nm), energy (eV), or wavenumber (cm^{-1}). The bandwidth and even the lineshape are different when different units are used. The bandwidth can be properly converted into different units. As an example, we consider a short pulse that has a spectral bandwidth in frequency as

$$\delta\nu = 5 \text{ THz}. \quad (1.15)$$

This bandwidth can be converted, for example, into units of angular frequency,

$$\delta\omega = 2\pi(\delta\nu) = 3.14 \times 10^{13} \text{ rad/s}, \quad (1.16)$$

wavenumber,

$$\delta\kappa = \frac{(\delta\nu)}{c} = 167 \text{ cm}^{-1}, \quad (1.17)$$

energy,

$$\delta U = h(\delta\nu) = 20.7 \text{ meV}, \quad (1.18)$$

or wavelength,

$$\delta\lambda = \frac{\lambda^2}{c}(\delta\nu), \quad (1.19)$$

where the last of these expressions is wavelength dependent. Assuming a wavelength of 800 nm, we have $\delta\lambda \approx 10$ nm.

10 Basics of ultrafast spectroscopy

Considering the intensity pulse duration $\delta t_{\text{FWHM}} = \sqrt{2 \ln 2} (\delta t_{e2})$, the pulse duration and the spectral bandwidth are related as $\delta t_{\text{FWHM}} = 4 \ln 2 / (\delta \omega_{\text{FWHM}})$. Therefore, a shorter pulse in the time domain requires a broader spectrum in the frequency domain and vice versa. The shortest possible pulse for a given bandwidth, known as the Fourier transform-limited pulse, can be achieved when the spectral phase is constant across the spectrum. The product of the bandwidth and the temporal duration of a pulse is a dimensionless number known as the time-bandwidth product (TBP). The TBP has a minimum value for a transform-limited pulse and the exact value depends on the pulse shape. If consistent units are used for time and bandwidth, the TBP is a unitless number. For example, a transform-limited Gaussian pulse has a TBP of $(\delta t_{\text{FWHM}})(\delta \nu_{\text{FWHM}}) = 0.441$ while the TBP is $(\delta t_{\text{FWHM}})(\delta \nu_{\text{FWHM}}) = 0.315$ for a transform-limited sech^2 -shaped pulse. These relations imply that 100-fs Gaussian pulses must have a bandwidth of 4.41 THz while 100-fs sech^2 -shaped pulses need a minimum bandwidth of 3.15 THz.

A pulse can have a carrier frequency that varies in time, in which case the pulse is called a chirped pulse. A linearly chirped Gaussian pulse can be written as

$$E(t) = E_0 e^{-\frac{t^2}{(\delta t_{e2})^2}} e^{-i(\omega_c t + \beta t^2)}, \quad (1.20)$$

where ω_c is the carrier frequency and βt^2 is the chirp. The term βt^2 modifies the carrier frequency and varies with time. It can be considered as a second-order phase. When β is positive, the pulse increases its frequency linearly in time (from red to blue) and is positively chirped. When β is negative, the pulse decreases its frequency linearly in time (from blue to red) and is negatively chirped.

Fourier transforming Eq. (1.20) gives the frequency-domain expression of the chirped pulse,

$$\mathcal{E}(\omega) = E_0 e^{-\frac{1/4}{(\delta \omega_{e2}/2) - i\beta} (\omega - \omega_c)^2} = E_0 e^{-\frac{(\delta \omega_{e2}/2)/4}{(\delta \omega_{e2}/2)^2 + \beta^2} (\omega - \omega_c)^2} e^{-i \frac{\beta/4}{(\delta \omega_{e2}/2)^2 + \beta^2} (\omega - \omega_c)^2}, \quad (1.21)$$

with $\delta \omega_{e2} = 2/(\delta t_{e2})$. Adding a chirp in the time domain changes the spectral width but not the temporal width of the pulse, while adding a chirp in the frequency domain changes the temporal width but not the spectral width of the pulse. In an experiment, a chirp is usually created by propagating through a dispersive medium, which is to say that the chirp is added in the frequency domain. As a result, in experiments, adding chirp typically results in increasing the temporal width of the pulses.

1.3 Ultrafast nonlinear/coherent spectroscopy

Ultrafast pulses enable unique capabilities in spectroscopy. First, the time resolution provided by ultrafast pulses can probe events that occur on fs to ps timescales. Second, the high instantaneous power and hence the strong electric field in ultrafast pulses can lead to more efficient nonlinear effects for nonlinear spectroscopy. Finally, a proper pulse sequence can be used to perform coherent spectroscopy. Incoherent spectroscopy, such as time-resolved fluorescence/luminescence and transient absorption spectroscopy, is only sensitive to population relaxation and the results can be interpreted by modeling with rate equations. In contrast, coherent spectroscopy, such

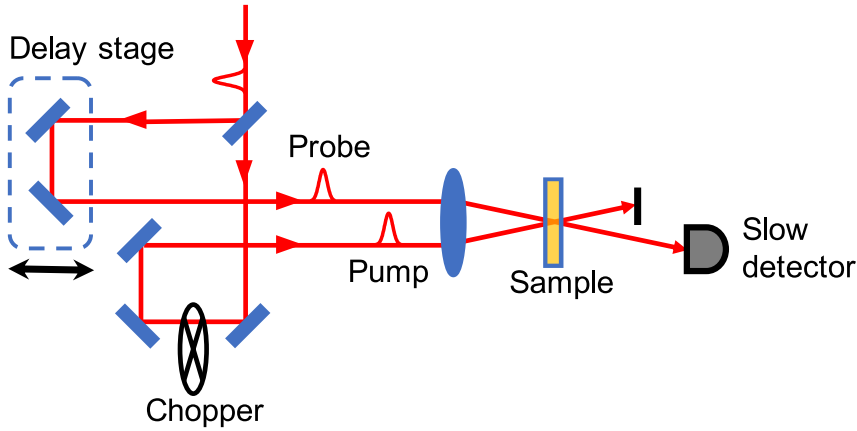


Fig. 1.3 Schematic of a typical pump-probe setup with two pulses and lock-in detection.

as transient four-wave mixing and multidimensional coherent spectroscopy, also probes phase relaxation and interpreting coherent spectra requires optical Bloch equations.

The simplest ultrafast technique is time-resolved fluorescence/luminescence spectroscopy. The technique uses only one pulse to excite the sample from the ground state to a high-lying excited state. The sample then relaxes to a lower excited state from which a fluorescence signal is spontaneously emitted. The fluorescence has a longer wavelength than the pump pulse so the signal can be distinguished from scattered pump photons. The signal can be recorded as a function of time by using time-resolved detection such as time-correlated photon counting or a streak camera, which has a typical time resolution of a few ps. The time resolution can be improved by cross correlating the fluorescence signal and a reference pulse through an upconversion nonlinear process, in which case the time resolution is only limited by the pulse duration. The measured fluorescence signal usually rises initially and then decays exponentially. The rise time of fluorescence is related to the relaxation time from the high-lying state to the lower excited state, while the decay dynamics are determined by the relaxation from the lower excited state to the ground state.

Pulse duration-limited time resolution can also be achieved by using a slow detector in the two-pulse transient absorption technique (also known as pump-probe). A typical pump-probe setup is depicted in Fig. 1.3. The sample is first excited by a pump pulse and the change in absorption due to excitation created by the pump pulse is measured using a subsequent probe pulse. Typically the absorption decreases after the pump pulse due to bleaching of the transition by the pump-induced population of excited states and depletion of the ground state population. As the population relaxes from the excited state back into the ground state, the absorption will recover, which is monitored by changing the delay between pump and probe pulses. The time delay between the pump and probe pulses can be varied by translating a mirror or retroreflector using a delay stage, thereby changing the path length and hence time delay due to the changed time-of-flight. The average power of the transmitted probe pulse is measured by a slow

detector. The change in the probe power due to the excitation by the pump is detected by using a lock-in amplifier as the pump beam is modulated by a optical chopper. The signal is recorded as a function of the time delay between the pump and probe pulses. The time resolution is determined by the minimum increment of the delay stage and the pulse duration. Assume that the unexcited sample has an absorption coefficient α_0 and the absorption coefficient decreases by $\Delta\alpha_0$ immediately after the excitation. For an excited state that decays exponentially with an excited-state lifetime of τ_{ex} , the change in the absorption coefficient at a delay time τ is given by

$$\Delta\alpha(\tau) = \Delta\alpha_0 e^{-\tau/\tau_{ex}}. \quad (1.22)$$

So the transmitted probe intensity and hence the average power depend on the delay τ and the lifetime τ_{ex} as

$$\begin{aligned} I_{tran}(\tau) &= I_{inc} e^{-[\alpha_0 - \Delta\alpha_0 e^{-\tau/\tau_{ex}}]L} \\ &\approx I_{tran}(0)(1 + \Delta\alpha_0 e^{-\tau/\tau_{ex}} L), \end{aligned} \quad (1.23)$$

where I_{inc} and I_{tran} are the incident intensity and the transmitted intensity, respectively, L is the sample length, and we assume $\Delta\alpha_0 L \ll 1$. The differential transmission, i.e., the relative change in transmitted intensity, or differential transmission, is

$$\begin{aligned} \frac{\Delta T(\tau)}{T_0} &= \frac{I_{tran}(\tau) - I_{tran}(0)}{I_{tran}(0)} \\ &\approx \Delta\alpha_0 e^{-\tau/\tau_{ex}} L, \end{aligned} \quad (1.24)$$

where T_0 is the transmission of unexcited sample and $\Delta T(\tau)$ is the change in the transmission at a delay τ . In the simplest case, the pump-probe signal features an exponential decay and measures the population decay dynamics of the pump-induced excitations. The pump-probe signal can be complicated in samples with more complex decay dynamics, for example, systems with multiple decay channels or intermediate states. The temporal behavior can deviate from a single exponential decay function and the differential transmission can even be negative. In the frequency-resolved version of pump-probe spectroscopy, known as spectrally resolved transient absorption, the transmitted probe is analyzed with a spectrometer to measure the wavelength dependence of the change in probe pulse. Spectral resolution can give more insight into the origin of the signal itself as well as helping to identify the reason for non-exponential dynamics.

A common coherent spectroscopic technique is transient four-wave mixing (TFWM), which can be performed with two or three pulses. The basic geometry for a two-pulse TFWM experiment is sketched in Fig. 1.4(a). Two pulses with wavevectors \mathbf{k}_1 and \mathbf{k}_2 are incident on the sample. The delay between the two pulses is τ and it is defined to be positive when pulse \mathbf{k}_1 arrives first. The nonlinear interaction gives rise to a TFWM signal in the direction $\mathbf{k}_s = 2\mathbf{k}_2 - \mathbf{k}_1$. A three-pulse TFWM experiment can be configured in different geometries. A planar geometry is shown in Fig. 1.4(b). The generated TFWM signal can be emitted in the direction $\mathbf{k}_s = -\mathbf{k}_1 + \mathbf{k}_2 + \mathbf{k}_3$. In the two-pulse and planar three-pulse geometries, it might be difficult to align the detector